

# Beyond Full Label: Single-Point Prompt for Infrared Small Target Label Generation

Shuai Yuan<sup>1,2</sup>, Hanlin Qin<sup>1</sup>, Renke Kou<sup>3</sup>, Xiang Yan<sup>1</sup>, Zechuan Li<sup>4</sup>,  
Chenxu Peng<sup>5</sup>, Abd-Krim Seghouane<sup>2</sup>

<sup>1</sup>College of Optoelectronic Engineering, Xidian University, Xi'an, China

<sup>2</sup>College of Mathematics and Statistics, The University of Melbourne, Parkville VIC 3052, Australia

<sup>3</sup>Shijiazhuang Campus, Army Engineering University, Shijiazhuang, China

<sup>4</sup>College of Electrical and Information Engineering, Hunan University, Changsha, China

<sup>5</sup>Zhejiang SUPCON Information Co. Ltd., Hangzhou, China

yuansy@stu.xidian.edu.cn, hlqin@mail.xidian.edu.cn, krk\_optics@aeu.edu.cn, xyan@xidian.edu.cn,

lizechuan@hnu.edu.cn, chenxupeng@gmail.com, karim.seghouane@gmail.com

## Abstract

In this work, we make the first attempt to construct a learning-based single-point annotation paradigm for infrared small target label generation (IRSTLG). Our intuition is that label generation requires just one more point prompt than target detection: IRSTLG can be regarded as an infrared small target detection (IRSTD) task with the target location hint. Based on this insight, we introduce an energy double guided single-point prompt (EDGSP)<sup>1</sup> framework, which adeptly transforms the target detection network into a refined label generation method. Specifically, the proposed EDGSP includes: 1) target energy initialization (TEI) to create a foundational outline for sufficient shape evolution of pseudo label, 2) double prompt embedding (DPE) for rapid localization of interested regions and reinforcement of individual differences to avoid label adhesion, and 3) bounding box-based matching (BBM) to eliminate false alarms. Experimental results show that pseudo labels generated by three baselines equipped with EDGSP achieve 100% object-level probability of detection ( $P_d$ ) and 0% false-alarm rate ( $F_a$ ) on SIRST, NUDT-SIRST, and IRSTD-1k datasets, with a pixel-level intersection over union (IoU) improvement of 13.28% over state-of-the-art label generation methods. Additionally, the downstream detection task reveals that our centroid-annotated pseudo labels surpass full labels, even with coarse single-point annotations, it still achieves 99.5% performance of full labeling.

## Introduction

Single-frame infrared small target detection (IRSTD) plays a crucial role in maritime rescue, early warning, and high-precision navigation (Wang, Zhou, and Wang 2019; Kou et al. 2023a,b; Zhang et al. 2024b). To isolate small targets from complex clutter, high-performance IRSTD methods typically extract discriminative features from extensive paired infrared images and pixel-level masks (Zhang et al. 2022; Wu et al. 2023; Chen et al. 2024a). This learning paradigm highlights the need for large-scale, accurate mask annotation. However, infrared (IR) small targets typically occupy only a few pixels, exhibit a low signal-to-clutter ratio, and lack well-defined edges. These characteristics render manual pixel-by-pixel annotation time-consuming and

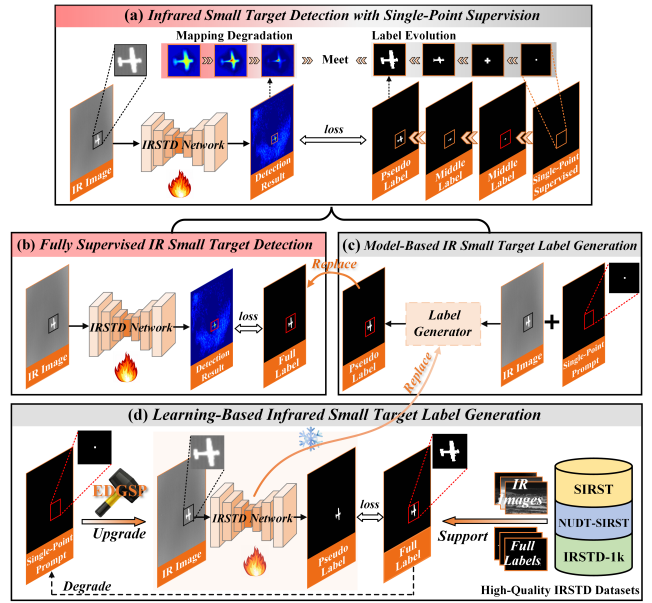


Figure 1: Task correlation between (a) single-point supervised IRSTD, (b) fully supervised IRSTD, (c) model-based IRSTLG, and (d) proposed learning-based IRSTLG.

error-prone. Consequently, an efficient and reliable infrared small target label generation (IRSTLG) method is urgently required.

Single-point annotation<sup>2</sup> (SA) has recently demonstrated efficiency in labeling IR small targets, reducing the time needed by 80% compared to pixel-level annotation. As shown in Figure 1(a), LESPS (Ying et al. 2023) made the first attempt to adopt SA for weakly supervised IRSTD. The mapping degradation is cleverly introduced to extract the target contour during network training. Then, these intermediate predictions are employed to guide the point label evolution. Precisely, LESPS integrates IRSTD network training with label generation into a unified framework. Subsequently, a standardized label generation paradigm emerged. As illustrated in Figure 1(c), these pioneering works use

<sup>1</sup>Code will be made public at <https://github.com/xdFai>.

<sup>2</sup>Unless explicitly stated, centroid single-point is used.

SA to guide traditional model optimization for generating pseudo masks, such as MCLC (Li et al. 2023a), MCGC (Kou et al. 2024), and COM (Li et al. 2024). Note that while these three works are claimed as “Single-Point Supervision”, they fundamentally belong to the label generation task with the single-point prompt as input. To avoid confusion, Figure 1(a)-(c) elucidates two critical links between these tasks. 1) If replace the full label in IRSTD with the pseudo label obtained in IRSTLG, *single-point supervised IRSTD can be treated as an organic combination of single-point prompt IRSTLG and fully supervised IRSTD*. This implies that developing IRSTLG can directly improve point-supervised IRSTD. 2) Label generation requires just one more point prompt than detection. Thus, *IRSTLG can be regarded as an infrared small target detection task with target location hint*. This indicates that the labeling task adheres to at least two essential criteria.

- The pseudo label should satisfy accurate annotation (AA), *i.e.*, object-level  $P_d=100\%$ ,  $F_a=0\%$ .
- IRSTLG frees up more effort to specialize in target contour than IRSTD, therefore should have higher IoU.

To validate this reasoning, Figure 2 showcases a comparison between the detection results of five IRSTD methods (Wu et al. 2023; Hou et al. 2022; Li et al. 2022; Wu, Hong, and Chanussot 2022; Yuan et al. 2024) with the pseudo masks generated by three IRSTLG algorithms (Li et al. 2023a; Kou et al. 2024; Li et al. 2024). Experimental results indicate that existing IRSTLG methods fail to meet standards in AA and IoU. This issue arises because these traditional algorithms neglect to leverage target location cues to extract features from fully labeled data.

Since well-designed IRSTD networks already achieve satisfactory target shape inference, and single-point prompts can be easily extracted from full labels, the primary goal of this paper is to design an effective “*Upgrade Tool*” that transforms the IRSTD network into a label generation method using the single-point prompt. As shown in Figure 1(d), the essence of this paradigm is *learning point prompt-based mask labeling experience from already labeled data*. In fact, point prompt combined with segmentation baseline has been applied to interactive annotation for general objects (Wang et al. 2019; Zhai et al. 2023). A common approach involves using multiple extreme points or corners to precisely crop the target region, then pairing it with the encoded prompt and full labels for fully supervised training. Although this pipeline has yielded satisfactory results in routine areas, directly applying it to our task reveals three pitfalls. 1) *Missing edge coordinates*. Only one pixel of the small target is annotated, the lack of edge coordinates hinders deep models focusing on the target contour. Even with multiple cropping scales and carefully crafted prompts, it still encounters obstacles in achieving accurate annotation (detailed see Experiments). 2) *Unique target characteristics*. Infrared small targets occupy only 0.15% of the total image pixels, and their edges are blurred by diffraction effects (Kou et al. 2023a). Two small targets in close proximity are easy to stick together and be mistakenly labeled as a single target, reducing  $P_d$ . 3) *Strong background clutter*.

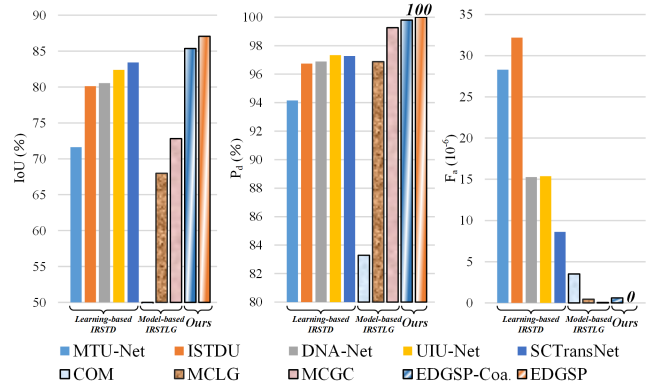


Figure 2: Comparing IRSTD and IRSTLG methods on mixed SIRST, NUDT-SIRST, and IRSTD-1k in  $IoU$  (%),  $P_d$  (%),  $F_a$  ( $10^{-6}$ ). *EDGSP-Coa.* denotes EDGSP with the coarse single-point prompt.

*ter.* Cloud edges, sea phosphorescence, and bright buildings in IR images have similar energy distributions to small targets (Zhang et al. 2024a). Even under effective location cues, this similarity still causes the deep model to misclassify pixels in these interference regions, resulting in false alarms.

To tackle these problems, we propose a novel framework for IRSTLG, named energy double guided single-point prompt (EDGSP). Without requiring complex cropping, EDGSP enables end-to-end model target contours through the integration of local and global context provided by the point prompt and deep model. As shown in Figure 3, this framework consists of three key components. 1) *Target energy initialization* (TEI): Inspired by IR targets that always have similar energy and shape distribution, we expand each point prompt into a Gaussian with local salience priors as the initial pattern of every target to evolve more complete outlines. 2) *Double prompt embedding* (DPE): The encoded prompt is embedded twice. The first embedding ensures the model directly focuses on the interested region, even in shallow layers. The second embedding refines the target salience map, enhancing target boundaries and preventing shape merging. 3) *Bounding box-based matching* (BBM): As a post-processing approach, we generate bounding boxes for each candidate target, then match the point prompt with each box by coordinates to eliminate clutter.

Benefiting from the above structures, as shown in Figure 2, our annotation method showcases powerful shape prediction capabilities and achieves  $P_d=100\%$ ,  $F_a=0\%$  on three datasets. The main contributions are summarised as follows.

- To the best of our knowledge, we present the first study of the learning-based IRSTLG paradigm, and introduce EDGSP creating a crucial link between label generation and target detection task.
- We propose the target energy initialization (TEI), double prompt embedding (DPE), and bounding box-based matching (BBM) strategies to address the insufficient label shape evolution, label adhesion, and false alarm.
- For the first time, three baselines equipped with EDGSP achieve accurate annotation on three datasets. The downstream detection task illustrates that our pseudo label sur-

passes the full label. Even with coarse point annotated, EDGSP achieves 99.5% performance of full labeling.

## Related Work

### Infrared Small Target Detection

IRSTD techniques have been developed over decades, and for a long period, they relied on handcrafted traditional methods such as image filtering (Bai and Zhou 2010; Deshpande et al. 1999), human visual system (Kim and Lee 2012; Chen et al. 2013), and low-rank optimization (Gao et al. 2013; Liu et al. 2023). Recently, deep learning-based methods have been able to obtain high-level semantics from large amounts of paired data by stacking nonlinear feature extractors, achieving robust detection in complex scenes. Since pixel-by-pixel classification is crucial for subsequent target recognition, segmentation-based IRSTD is a key emphasis in these data-driven approaches. Based on a U-shaped structure (Ronneberger, Fischer, and Brox 2015), ACM (Dai et al. 2021) improves the feature fusion strategy of high-level semantics with low-level details using an asymmetric context modulator. To mitigate the semantic gap between encoders and decoders, DNA-Net (Li et al. 2022) adopts dense nested interactive modules to facilitate progressive interaction of cross-scale features and adaptive enhancement of fine-grained features, while UIU-Net (Wu, Hong, and Chanussot 2022) directly nest multiple small U-Net into each codec of U-shaped structure. To address the limitations in long-range information modeling, MTU-Net (Wu et al. 2023) employs a self-attention to compute the spatial correlations of fused features, thereby constructing a global representation of the image. Most recently, SCTransNet (Yuan et al. 2024) explicitly interacts and enhances full-level encoder features by spatial-channel cross transformer blocks to effectively suppress interference.

In summary, existing research emphasizes designing tight structures to achieve high performance. However, the labor-intensive task of pixel-by-pixel annotation for infrared small targets hampers the advancement of these data-dependent methods. Therefore, this work aims to alleviate the burden of infrared small target labeling.

### Point Supervised Segmentation

One working mode related to us is point-supervised segmentation. As a weak supervision form, point supervision only requires one or a few points as label (Qian et al. 2019; Zhao and Yin 2020; Li et al. 2023b). Bearman et al. (Bearman et al. 2016) propose the first single-point supervised semantic segmentation method by integrating an objectiveness prior into a loss function, to elevate segmentation effectiveness. Subsequently, Zhang et al. (Zhang et al. 2023) leverage the common characteristics of target regions and present a contrast-based variational model for point-supervised histopathology image segmentation, achieving more regionally consistent and smoother boundaries. Close to our work, LESPS (Ying et al. 2023) is the first to introduce single-point supervision to infrared small target detection task, based on mapping degradation phenomenon to guide point label evolution.

Unlike the aforementioned works, we still rely on fully annotated masks for supervision, yet employ single-point as a form of input to guide the IRSTD network. This approach reveals how to utilize additional prompts to achieve high-precision pseudo-label generation for small targets.

### Infrared Small Target Label Generation

To the best of our knowledge, there are only three IRSTLG efforts. They are all based on the model-based single-point prompt methods. As a pioneer, MCLC (Li et al. 2023a) makes the first attempt to employ a Monte Carlo linear clustering process with random noise and averages the clustering results to obtain reliable pseudo masks. Subsequently, MCGC adaptive recovers small targets with multi-scale chain growth clustering, further enhancing annotation robustness (Kou et al. 2024). Recently, Li et al. (Li et al. 2024) designed a variational level set with an expected difference energy function to address the excessive regularization causing target contours to disappear. However, these works tend to treat the points as a "Supervision" signal. This biased task orientation causes them to overlook the potential of combining point prompt-derived location cues to extract features from complete labeled datasets, culminating in pseudo labels with unclear edges, target adhesion, and false alarms.

In this paper, we accurately define the operating paradigm where images and single-point prompts serve as inputs and produce pseudo labels as "single-point prompt for infrared small target label generation". Unlike previous methods, we present the first study of a learning-based paradigm for IRSTLG, which artfully evolves the target detection network into an advanced label generation method with the aid of the single-point prompt.

### Point Prompt Interactive Segmentation

The technique most similar to ours is point prompt interactive segmentation (Rother, Kolmogorov, and Blake 2004; Xu et al. 2016; Liew et al. 2017), which aims to reduce annotation time. DEXTR (Maninis et al. 2018) uses four extreme points for segmentation, the interest region is cropped and the Gaussian heat map is utilized as the encoding form of prompts. Similarly, IOG (Zhang et al. 2020) uses the approximate center of the target as the inside point and a set of symmetrical corner points as the outside points. After cropping the target of interest, the image, along with heat maps is fed into the segmentation model. Luo et al. (Luo et al. 2021) uses the exponentialized geodesic distance transform to convert medical images into Euclidean distance maps for improved foreground-background separation. Recently, SAM (Kirillov et al. 2023) has gained recognition for its flexibility and generalization capabilities. It is a transformer-based model for semantic segmentation that utilizes various types of prompts to encode key areas.

Despite the success of the above work on generic target segmentation, the unique characteristics and annotation patterns of infrared small targets render these strategies ineffective. The proposed EDGSP differs from them in three ways: 1) It processes the entire image directly without cropping. 2) It assigns explicit physical meaning to Gaussian heat maps, thereby using the double embedding strategy. 3) EDGSP

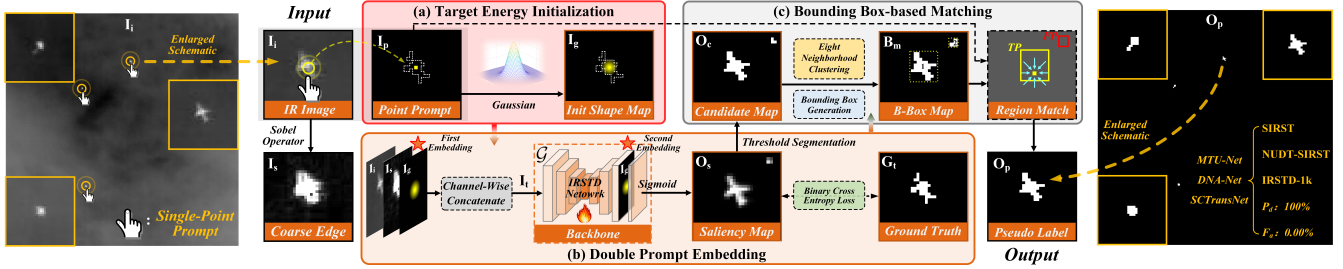


Figure 3: Illustration of the proposed energy double guided single-point prompt (EDGSP) framework. It consists of three parts. (a) Target energy initialization (TEI) for sufficient shape evolution, (b) double prompt embedding (DPE) to reinforce individual differences and prevent mask adhesion, and (c) bounding box-based matching (BBM) to eliminate false alarms.

introduces a box-based matching approach specifically designed to eliminate false alarms.

## Proposed Method

The overview of our proposed EDGSP is shown in Figure 3. It is very concise and consists of three parts.

### Target Energy Initialization

The long-range imaging mechanism of infrared systems brings severe diffraction effects, resulting in small targets appearing with a nearly Gaussian distribution in infrared images (Dai et al. 2023). By combining this physical phenomenon with the local contrast prior of small targets (Chen et al. 2013), we propose target energy initialization to predefine a basic profile for each target. As shown in Figure 3, given an input image  $\mathbf{I}_i \in \mathbb{R}^{1 \times H \times W}$  and corresponding single-point prompt  $\mathbf{I}_p \in \mathbb{R}^{1 \times H \times W}$  (Since the single-point prompt is a pixel within the target, it can be derived from the already labeled ground truth  $\mathbf{G}_t \in \mathbb{R}^{1 \times H \times W}$ ). 2D Gaussian function is used to expand each point in  $\mathbf{I}_p$  as an energy blob, thus creating a single init shape map  $\mathbf{I}_g \in \mathbb{R}^{1 \times H \times W}$ . This expansion simplifies the task by shifting from shaping area targets with points to refining contours using Gaussian blobs, aligning the prior distribution of the targets, and aiding the model in learning complete shape representations.

### Double Prompt Embedding

Without loss of generality, given a U-shaped IRSTD network  $\mathcal{G}$ , encoded prompt  $\mathbf{I}_g$  embed into  $\mathcal{G}$  twice, as shown in Figure 3(b). Considering that edge information can guide shape construction (Zhang et al. 2022), the Sobel operator  $\mathcal{S}$  is first applied to the original infrared image  $\mathbf{I}_i$  to obtain a rough edge map  $\mathbf{I}_s$ . Then,  $\mathbf{I}_i$ ,  $\mathbf{I}_s$ , and the init shape map  $\mathbf{I}_g$  are concatenated among the channel dimension as a three-channel input image  $\mathbf{I}_t \in \mathbb{R}^{3 \times H \times W}$ , and get the penultimate layer features  $\mathbf{L}$  of  $\mathcal{G}$  as follows:

$$\mathbf{I}_t = \text{Concat}(\mathbf{I}_i, \mathcal{S}(\mathbf{I}_i), \mathbf{I}_g) \quad (1)$$

$$\mathbf{L} = \mathcal{G}_{w/o}^{\text{Conv}}(\mathbf{I}_t) \quad (2)$$

where  $\mathcal{G}_{w/o}^{\text{Conv}}$  stands for  $\mathcal{G}$  that without the last convolution layer. In the second embedding,  $\mathbf{I}_g$  is treated as a semantic map that reinforces the target quantity, it is concatenated

with the  $\mathbf{L}$  along the channel dimension to refine the model’s final mapping and prevent close-range target sticking.

$$\mathbf{O}_s = \text{Sigmoid}(\text{Conv}(\text{Concat}(\mathbf{L}, \mathbf{I}_g))) \quad (3)$$

where  $\mathbf{O}_s \in \mathbb{R}^{1 \times H \times W}$  represents the saliency map,  $\text{Conv}$  denotes the last layer of  $\mathcal{G}$ , typically constructed with a  $1 \times 1$  or  $3 \times 3$  convolution that squeezes channel and preserves the spatial dimensions. The binary cross entropy loss is then used to compute pixel-wise differences between the  $\mathbf{O}_s$  and the ground truth  $\mathbf{G}_t$ .

### Bounding Box-based Matching

In previous works, eight connective regions matching is popular to eliminate false alarms during the label evolution process (Ying et al. 2023; Kou et al. 2024), ensuring that evolution information consistently applies to the initial point. However, this strategy ignores cases where the point prompt is located on or outside the target boundary, leading to incorrect processing results<sup>3</sup>. We tackle this issue by adding a compact design. In Figure 3(c), after performing eight-neighborhood clustering on the threshold-segmented candidate map  $\mathbf{O}_c$ , we generate bounding boxes for each component to create a b-box map  $\mathbf{B}_m$ . Then, match the point prompt  $\mathbf{I}_p$  with  $\mathbf{B}_m$ . Specifically, if the point in  $\mathbf{I}_p$  falls inside a bounding box, the target in this box is retained; otherwise, it is discarded as a false positive. After performing this region match, we got the final pseudo label  $\mathbf{O}_p$ .

## Experiments

### Experimental Setup

**Datasets.** Experiments are conducted on three mixed datasets: SIRST (Dai et al. 2021), NUDT-SIRST (Li et al. 2022), and IRSTD-1k (Zhang et al. 2022), which include 427, 1327, and 1001 infrared images with one or more targets, respectively. We used the method from (Li et al. 2022) to partition the datasets for SIRST and NUDT-SIRST, and followed (Zhang et al. 2022) for splitting IRSTD-1k.

**Implement Details.** SCTransNet (Yuan et al. 2024) is used as the backbone of EDGSP. The peak half-width of the Gaussian is set to 4 and the segmentation threshold is set to 0.5. We compare all IRSTLG methods: MCLC (Li et al.

<sup>3</sup>The shortcomings of this approach are detailed in the supplementary material.

Table 1: Comparison with SOTA IRSTLG methods on SIRST, NUDT-SIRST, IRSTD-1k in terms of  $IoU(\%)$ ,  $P_d(\%)$ ,  $F_{at}(\%)$ ,  $F_a(10^{-6})$ . The best and the second-best results are highlighted in bold and underlined, respectively. *EDGSP-Coa.* indicates the EDGSP under the coarse single-point prompt.

Method	SIRST				NUDT-SIRST				IRSTD-1k				Total			
	$IoU \uparrow$	$P_d \uparrow$	$F_{at} \downarrow$	$F_a \downarrow$	$IoU \uparrow$	$P_d \uparrow$	$F_{at} \downarrow$	$F_a \downarrow$	$IoU \uparrow$	$P_d \uparrow$	$F_{at} \downarrow$	$F_a \downarrow$	$IoU \uparrow$	$P_d \uparrow$	$F_{at} \downarrow$	$F_a \downarrow$
LESPTS	41.84	97.71	1.52	0.27	38.86	98.94	0.95	2.06	38.76	98.98	0.68	0.04	39.28	98.73	1.00	0.14
COM	53.19	83.65	10.3	1.85	8.026	52.54	32.1	6.96	41.21	69.39	20.1	1.12	13.84	61.29	25.9	3.51
MCLC	75.63	98.48	3.80	0.68	65.08	95.87	12.2	2.64	69.60	98.64	4.42	0.25	67.98	96.87	9.19	1.25
MCGC	72.43	97.33	0.76	0.14	77.67	99.68	0.32	0.07	63.24	<u>99.66</u>	0.34	<u>0.02</u>	72.80	99.26	0.40	0.05
SAM	6.273	<b>100.0</b>	0.76	0.14	8.466	<b>100.0</b>	0.74	0.16	2.428	<b>100.0</b>	1.02	0.06	6.41	<b>100.0</b>	0.80	0.11
Robust SAM	78.89	98.86	<u>0.38</u>	0.07	67.05	99.79	0.21	<u>0.05</u>	<u>72.28</u>	99.32	<u>0.34</u>	<u>0.02</u>	70.14	99.53	0.27	<u>0.04</u>
EDGSP-Coa.	<u>83.05</u>	<u>99.62</u>	<b>0</b>	<b>0</b>	<u>94.23</u>	<u>99.89</u>	<u>0.11</u>	1.01	71.07	<u>99.66</u>	<u>0.34</u>	0.47	<u>85.36</u>	<u>99.80</u>	<u>0.13</u>	0.62
EDGSP	<b>83.83</b>	<b>100.0</b>	<b>0</b>	<b>0</b>	<b>95.51</b>	<b>100.0</b>	<b>0</b>	<b>0</b>	<b>73.80</b>	<b>100.0</b>	<b>0</b>	<b>0</b>	<b>87.07</b>	<b>100.0</b>	<b>0</b>	<b>0</b>

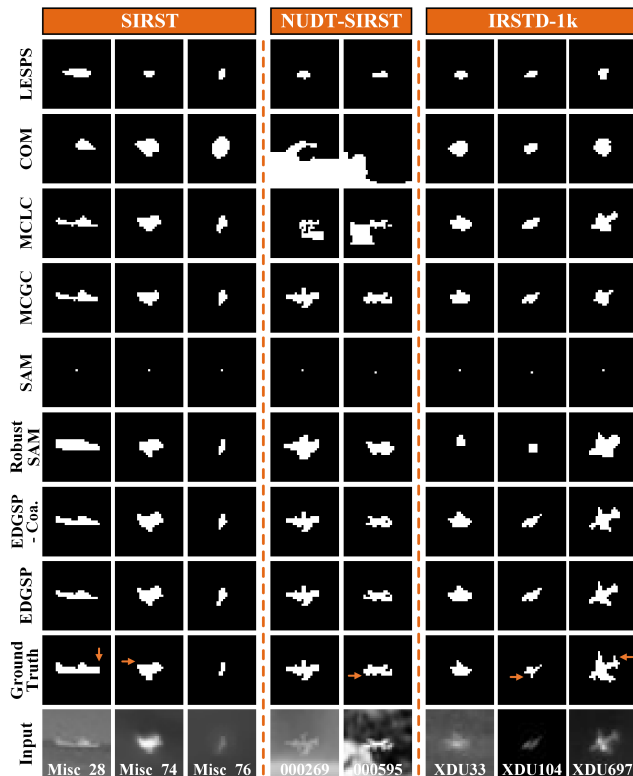


Figure 4: Visual results of seven IRSTLG methods on the SIRST, NUDT-SIRST, IRSTD-1k. *EDGSP-Coa.* denotes the pseudo label of EDGSP under coarse single-point prompt. Small flaws in ground truth are highlighted with arrows. Refer to supplementary material for more visual results.

2023a), MCGC (Kou et al. 2024) and COM (Li et al. 2024), and learning-based single-point annotation methods: SAM (Kirillov et al. 2023) and Robust SAM (Chen et al. 2024b). Furthermore, we also include the point-supervised IRSTD framework LESPTS (Ying et al. 2023), using DNA-Net as the backbone, consistent with the original paper. We provide more details of experiments in the supplementary

material.

**Evaluation Metrics.** To evaluate pseudo labels and downstream target detection results, intersection over union (IoU) is used as a pixel-level metric to assess the model’s contour inference capability (Dai et al. 2021). probability of detection ( $P_d$ ) and false-alarm rate ( $F_a$ ) are utilized as target-level evaluation metrics to assess localization capabilities. The details of  $P_d$ ,  $F_a$  are same as (Li et al. 2022). Considering the number of false alarms is more important for the labeling task, the target false-alarm rate ( $F_{at}$ ) is defined as the ratio of false predicted target numbers  $T_{false}$  and all targets  $N_{all}$ .

## Quantitative Results

As shown in Table 1, only EDGSP achieves  $P_d=100\%$ ,  $F_a=0\%$ ,  $F_{at}=0\%$  across three datasets at the same time. This indicates that our framework is currently the only one ensuring the most basic level of annotation quality. Additionally, EDGSP’s IoU surpasses the state-of-the-art (SOTA) labeling method (MCGC) by 14.27, demonstrating a superior shape prediction capability. Even with the coarse single-point prompt, EDGSP outperforms other methods with the centroid single-point prompt.

## Qualitative Results

Figure 4 illustrates that the results of EDGSP are closer to the target silhouette in the infrared image than those of other models. In fact, many pseudo masks such as Misc\_28, Misc\_74, 000595, XDU104, and XDU697 even exceed the quality of ground truth (GT). We also observe that COM and MCLC tend to merge the target with the background, while LESPTS, MCGC, and Robust SAM struggle to accurately infer the morphology of infrared small targets. Additionally, SAM is incapable of labeling infrared small targets.

## Upgrade Tool: EDGSP

As shown in Table 2, with the help of EDGSP, the average IoU and  $P_d$  values for seven SOTA IRSTD methods, including ACM (Dai et al. 2021), ALCNet (Dai et al. 2021), MTU-Net (Wu et al. 2023), ISTDU (Hou et al.

Table 2: The improvement brought by the EDGSP framework to seven SOTA IRSTD methods on SIRST, NUDT-SIRST, IRSTD-1k in terms of  $IoU(\%)$ ,  $P_d(\%)$ ,  $F_{at}(\%)$ ,  $F_a(10^{-6})$ ,  $Flops(G)$ , and  $Params(M)$ .

Method	IRSTD Baseline						IRSTD with EDGSP					
	$IoU \uparrow$	$P_d \uparrow$	$F_{at} \downarrow$	$F_a \downarrow$	$Flops \downarrow$	$Params \downarrow$	$IoU \uparrow$	$P_d \uparrow$	$F_{at} \downarrow$	$F_a \downarrow$	$Flops \downarrow$	$Params \downarrow$
ACM	61.43	94.80	13.75	64.50	0.402	0.398	73.60	99.60	0.066	0.28	0.405	0.398
ALCNet	63.26	94.98	13.69	58.74	0.378	0.427	74.06	99.67	0.066	1.71	0.381	0.427
MTU-Net	71.62	94.15	12.16	28.31	6.194	8.221	84.20	100.0	0	0	6.215	8.221
ISTDU	80.12	96.74	9.103	32.18	7.944	2.752	84.07	99.93	0.066	1.11	7.973	2.752
DNA-Net	80.53	96.90	5.249	15.28	14.26	4.697	86.78	100.0	0	0	14.28	4.697
UIU-Net	82.40	97.34	6.389	15.39	54.43	50.54	86.96	99.93	0	0	54.50	50.54
SCTransNet	83.43	97.28	5.781	8.622	10.12	11.19	87.07	100.0	0	0	10.16	11.19
Average	73.81	95.79	9.993	34.32	13.39	11.18	82.19	99.85	0.041	0.43	13.42	11.18
Difference	-	-	-	-	-	-	<b>+8.38</b>	<b>+4.06</b>	<b><math>\times 0.35\%</math></b>	<b><math>\times 1.25\%</math></b>	<b>+0.04</b>	<b>+0</b>

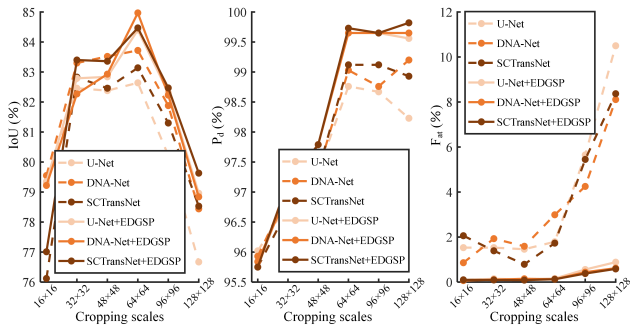


Figure 5: Quantitative results of three baselines at six cropping scales in terms of  $IoU(\%)$ ,  $P_d(\%)$ ,  $F_{at}(\%)$ . Dashed and solid lines represent label generation results from direct center-cropping and from using EDGSP on the cropped image, respectively.

2022), DNA-Net (Li et al. 2022), UIU-Net (Wu, Hong, and Chanussot 2022) and SCTRansNet (Yuan et al. 2024), improved by 8.38% and 4.06%, respectively, while the  $F_{at}$  decreased by a factor of 243.73. Flops and parameters remained nearly constant. Three IRSTD methods (MTU-Net, DNA-Net, and SCTRansNet) achieve accurate annotations. This indicates that EDGSP builds a reliable bridge between IRSTD and IRSTLG. We also found a positive correlation between pseudo-label performance and detection results, indicating that future iterations of the IRSTD method can further enhance pseudo-label quality through EDGSP. Given that SCTRansNet achieved the highest IoU score, we selected it as the backbone for EDGSP unless stated differently.

### Prompt-based Center-Cropping

Figure 5 showcases the results of three baselines (U-Net, DNA-Net, and SCTRansNet) under prompt-based center-cropping. With the crop size increasing, model performance initially improves and then declines, and fails to achieve high-performance labeling ( $P_d < 100\%$ ,  $IoU < 85$ ). This is because small crop sizes fail to encompass large targets,

Table 3: Based on SCTRansNet (SCT), ablation study of the single prompt embedding (SPE), TEI, rough edge map (REM), DPE, and BBM on SIRST, NUDT-SIRST, and IRSTD-1k. SPE means directly concatenating the single-point prompt with the original image as input. More details of each module are discussed in the supplementary material.

Method	SCT	SPE	TEI	REM	DPE	BBM	$IoU \uparrow$	$P_d \uparrow$	$F_{at} \downarrow$
M1	✓						83.43	97.28	5.78
M2	✓	✓					86.16	99.67	1.73
M3	✓	✓	✓				86.52	100.0	1.74
M4	✓	✓	✓	✓			86.74	99.93	1.93
M5	✓		✓	✓	✓		87.02	100.0	1.59
Ours	✓		✓	✓	✓	✓	87.07	100.0	0

while large crop sizes introduce excessive irrelevant padding at the image edges. Additionally, target overlap is challenging to manage when splicing the inferred image back into the original image. In summary, missing boundary coordinate information diminishes the effectiveness of the formal center-cropping strategy. Therefore, EDGSP directly processes the entire image.

### Ablation Study

As shown in Table 3, SCTRansNet is used as the baseline to validate the effectiveness of each proposed strategy. In M2, just incorporating single prompt embedding, the value of  $P_d$  and  $IoU$  exceeds the full cropping strategies in Figure 5, illustrating the necessity of entire image processing. Using SPE, the  $IoU$  value further improved, and  $P_d$  reached 100%, which demonstrated the SPE is capable of fleshing out target shapes and highlighting edge differences. The incorporation of the rough edge map raised the IOU further but led to target sticking. In M5, SPE is replaced with DPE. We can see that prompt embedding at the tail of the model enhances target edge differences again and improves overall perfor-

Table 4: Quantitative results of five IRSTD trained with five types of pseudo-labels and full labels on downstream test sets in terms of  $IoU$ (%),  $P_d$ (%),  $F_a$ (%). The best and the second-best results are highlighted in bold and underlined, respectively.

Method	Pseudo Label					Full Label
	MCLC	MCGC	Robust SAM	EDGSP-Coa.	EDGSP	
ACM	61.17/90.07/22.16	61.42/91.72/23.57	62.43/92.38/29.22	65.03/92.38/23.97	65.59/91.39/23.92	65.65/93.38/32.70
RDIAN	64.94/94.04/28.54	68.38/93.38/16.96	65.57/93.38/24.43	73.27/93.05/21.26	74.68/93.71/18.23	72.64/92.72/13.93
MTU-Net	66.33/89.07/18.00	68.24/93.71/10.49	66.54/93.38/20.36	75.46/93.38/9.95	75.31/95.36/17.96	75.89/94.70/13.48
DNA-Net	66.12/93.05/15.29	67.80/93.38/6.60	67.91/94.37/12.48	81.52/94.70/7.55	81.53/96.69/8.14	81.63/95.70/9.00
UIU-Net	66.07/93.05/44.06	69.55/93.71/4.26	66.57/93.70/6.02	81.14/94.70/8.73	82.70/96.03/6.02	82.46/96.68/7.46
Average	64.93/91.86/25.61	67.08/93.18/12.38	65.80/93.44/18.50	75.28/93.64/14.29	<b><u>75.96/94.64/14.85</u></b>	75.65/94.64/15.31

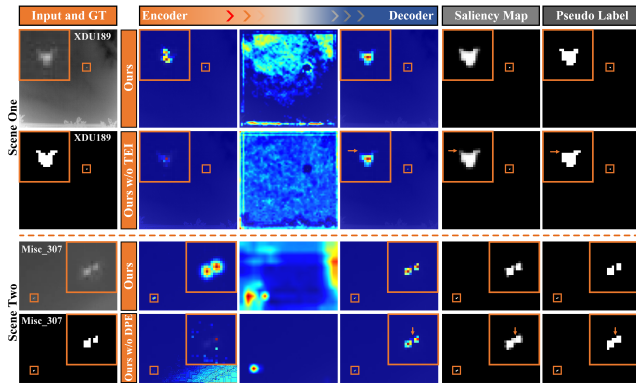


Figure 6: Visual maps of ablation study on TEI and DPE. Incomplete labeling and adhesion are highlighted with arrows.

mance. Finally, BBM accurately eliminates false alarms and EDGSP achieves accurate annotation. In Figure 6, with the help of target energy initialization, our model quickly responds to the target area and accurately predicts the left rotor of the drone. In scene two, without double prompt embedding (*Ours w/o DPE*), neighboring targets blend. We further observe that the attention map also responded in the background region, revealing that the local shape prediction remains connected to the global context modeling. This finding underscores again the importance of preserving the entire scene.

## Downstream IRSTD

We used the inferred pseudo masks<sup>4</sup> from the test sets of SIRST, NUDT-SIRST, and IRSTD-1k to train the detection model, to validate the effectiveness of the pseudo labels for downstream IRSTD. Quantitative results are shown in Table 4. EDGSP outperforms other single-point prompt label generation methods. Although MCGC achieves the lowest  $F_a$ , it also has a low IoU score. Remarkably, EDGSP not only reduces time cost by 80% but also outperforms full labels in detection task. Even with coarse point prompts, It

<sup>4</sup>The number of data is 1505, training and test sets split as 8:2, we performed three cross-validations.

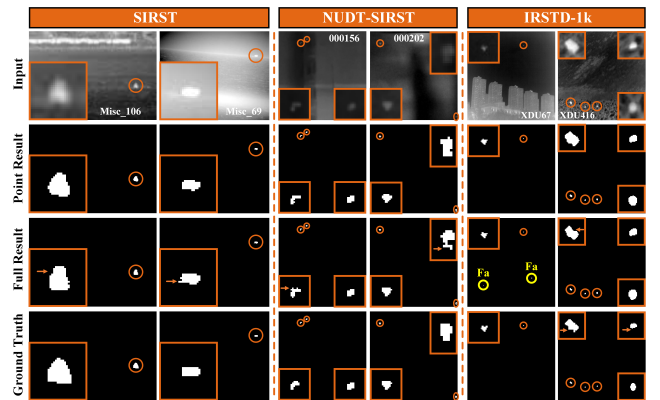


Figure 7: Visual results of DNA-Net. “Point Result” and “Full Result” indicate the outcomes of DNA-Net trained with the pseudo label from EDGSP and the full label, respectively. The correctly detected targets and false alarms are highlighted in orange and yellow circles, while incomplete shape inferences are marked with arrows.

still achieves 99.5% of the performance of full labels. Visual results are shown in Figure 7, compared to full labels, DNA-Net trained with EDGSP’s pseudo mask demonstrates enhanced shape inference and lower false alarm. This reaffirms the applicability of the proposed methodology.

## Conclusion

In this article, we propose a novel annotation paradigm: enhancing detection networks with single-point prompts to accomplish the high-level IRSTLG. Specifically, we introduce the energy double guided single-point prompt (EDGSP) framework. It includes target energy initialization for effective shape evolution, double prompt embedding to prevent label adhesion, and bounding box-based matching to eliminate false alarms. This framework achieves accurate annotation on the SIRST, NUDT-SIRST, and IRSTD-1k datasets for the first time, and demonstrates superior performance compared to full labels in downstream IRSTD. In the future, we will focus on the coarse single-point prompt IRSTLG to further improve the utility of this framework.

## References

- Bai, X.; and Zhou, F. 2010. Analysis of new top-hat transformation and the application for infrared dim small target detection. *Pattern Recognition*, 43(6): 2145–2156.
- Bearman, A.; Russakovsky, O.; Ferrari, V.; and Fei-Fei, L. 2016. What’s the point: Semantic segmentation with point supervision. In *European Conference on Computer Vision (ECCV)*, 549–565. Springer.
- Chen, C. P.; Li, H.; Wei, Y.; Xia, T.; and Tang, Y. Y. 2013. A local contrast method for small infrared target detection. *IEEE Transactions on Geoscience and Remote Sensing*, 52(1): 574–581.
- Chen, T.; Tan, Z.; Gong, T.; Chu, Q.; Wu, Y.; Liu, B.; Ye, J.; and Yu, N. 2024a. MiM-ISTD: Mamba-in-mamba for efficient infrared small target detection. *arXiv preprint arXiv:2403.02148*.
- Chen, W.-T.; Vong, Y.-J.; Kuo, S.-Y.; Ma, S.; and Wang, J. 2024b. RobustSAM: Segment Anything Robustly on Degraded Images. In *Proceedings of the IEEE/CVF Conference on Computer Vision and Pattern Recognition (CVPR)*, 4081–4091.
- Dai, Y.; Li, X.; Zhou, F.; Qian, Y.; Chen, Y.; and Yang, J. 2023. One-Stage Cascade Refinement Networks for Infrared Small Target Detection. *IEEE Transactions on Geoscience and Remote Sensing*, 1–17.
- Dai, Y.; Wu, Y.; Zhou, F.; and Barnard, K. 2021. Asymmetric contextual modulation for infrared small target detection. In *Proceedings of the IEEE/CVF Winter Conference on Applications of Computer Vision*, 950–959.
- Dai, Y.; Wu, Y.; Zhou, F.; and Barnard, K. 2021. Attentional local contrast networks for infrared small target detection. *IEEE Transactions on Geoscience and Remote Sensing*, 59(11): 9813–9824.
- Deshpande, S. D.; Er, M. H.; Venkateswarlu, R.; and Chan, P. 1999. Max-mean and max-median filters for detection of small targets. In *Signal and Data Processing of Small Targets 1999*, volume 3809, 74–83. SPIE.
- Gao, C.; Meng, D.; Yang, Y.; Wang, Y.; Zhou, X.; and Hauptmann, A. G. 2013. Infrared Patch-Image Model for Small Target Detection in a Single Image. *IEEE Transactions on Image Processing*, 22(12): 4996–5009.
- Hou, Q.; Zhang, L.; Tan, F.; Xi, Y.; Zheng, H.; and Li, N. 2022. ISTDU-Net: Infrared Small-Target Detection U-Net. *IEEE Geoscience and Remote Sensing Letters*, 19: 1–5.
- Kim, S.; and Lee, J. 2012. Scale invariant small target detection by optimizing signal-to-clutter ratio in heterogeneous background for infrared search and track. *Pattern Recognition*, 45(1): 393–406.
- Kirillov, A.; Mintun, E.; Ravi, N.; Mao, H.; Rolland, C.; Gustafson, L.; Xiao, T.; Whitehead, S.; Berg, A. C.; Lo, W.-Y.; Dollar, P.; and Girshick, R. 2023. Segment Anything. In *Proceedings of the IEEE/CVF International Conference on Computer Vision (ICCV)*, 4015–4026.
- Kou, R.; Wang, C.; Fu, Q.; Li, Z.; Luo, Y.; Li, B.; Li, W.; and Peng, Z. 2024. MCGC: A Multi-scale Chain Growth Clustering Algorithm for Generating Infrared Small Target Mask under Single-point Supervision. *IEEE Transactions on Geoscience and Remote Sensing*.
- Kou, R.; Wang, C.; Peng, Z.; Zhao, Z.; Chen, Y.; Han, J.; Huang, F.; Yu, Y.; and Fu, Q. 2023a. Infrared small target segmentation networks: A survey. *Pattern Recognition*, 143: 109788.
- Kou, R.; Wang, C.; Yu, Y.; Peng, Z.; Huang, F.; and Fu, Q. 2023b. Infrared small target tracking algorithm via segmentation network and multistrategy fusion. *IEEE Transactions on Geoscience and Remote Sensing*, 61: 1–12.
- Li, B.; Wang, Y.; Wang, L.; Zhang, F.; Liu, T.; Lin, Z.; An, W.; and Guo, Y. 2023a. Monte Carlo linear clustering with single-point supervision is enough for infrared small target detection. In *Proceedings of the IEEE/CVF International Conference on Computer Vision (ICCV)*, 1009–1019.
- Li, B.; Xiao, C.; Wang, L.; Wang, Y.; Lin, Z.; Li, M.; An, W.; and Guo, Y. 2022. Dense nested attention network for infrared small target detection. *IEEE Transactions on Image Processing*, 32: 1745–1758.
- Li, H.; Yang, J.; Xu, Y.; and Wang, R. 2024. A Level Set Annotation Framework with Single-Point Supervision for Infrared Small Target Detection. *IEEE Signal Processing Letters*.
- Li, Y.; Zhao, H.; Qi, X.; Chen, Y.; Qi, L.; Wang, L.; Li, Z.; Sun, J.; and Jia, J. 2023b. Fully Convolutional Networks for Panoptic Segmentation With Point-Based Supervision. *IEEE Transactions on Pattern Analysis and Machine Intelligence*, 45(4): 4552–4568.
- Liew, J.; Wei, Y.; Xiong, W.; Ong, S.-H.; and Feng, J. 2017. Regional interactive image segmentation networks. In *2017 IEEE International Conference on Computer Vision (ICCV)*, 2746–2754. IEEE.
- Liu, Y.; Liu, X.; Hao, X.; Tang, W.; Zhang, S.; and Lei, T. 2023. Single-Frame Infrared Small Target Detection by High Local Variance, Low-Rank and Sparse Decomposition. *IEEE Transactions on Geoscience and Remote Sensing*, 61: 1–17.
- Luo, X.; Wang, G.; Song, T.; Zhang, J.; and Zhang, S. 2021. MIDeepSeg: Minimally Interactive Segmentation of Unseen Objects from Medical Images Using Deep Learning. *Medical Image Analysis*.
- Maninis, K.-K.; Caelles, S.; Pont-Tuset, J.; and Van Gool, L. 2018. Deep extreme cut: From extreme points to object segmentation. In *Proceedings of the IEEE/CVF Conference on Computer Vision and Pattern Recognition (CVPR)*, 616–625.
- Qian, R.; Wei, Y.; Shi, H.; Li, J.; Liu, J.; and Huang, T. 2019. Weakly supervised scene parsing with point-based distance metric learning. In *Proceedings of the AAAI Conference on Artificial Intelligence*, volume 33, 8843–8850.
- Ronneberger, O.; Fischer, P.; and Brox, T. 2015. U-Net: Convolutional networks for biomedical image segmentation. In *Medical Image Computing and Computer-Assisted Intervention—MICCAI 2015: 18th International Conference, Munich, Germany, October 5-9, 2015, Proceedings, Part III* 18, 234–241. Springer.



- Rother, C.; Kolmogorov, V.; and Blake, A. 2004. "GrabCut" interactive foreground extraction using iterated graph cuts. *ACM transactions on graphics (TOG)*, 23(3): 309–314.
- Wang, G.; Zuluaga, M. A.; Li, W.; Pratt, R.; Patel, P. A.; Aertsen, M.; Doel, T.; David, A. L.; Deprest, J.; Ourselin, S.; and Vercauteren, T. 2019. DeepIGeoS: A Deep Interactive Geodesic Framework for Medical Image Segmentation. *IEEE Transactions on Pattern Analysis and Machine Intelligence*, 41(7): 1559–1572.
- Wang, H.; Zhou, L.; and Wang, L. 2019. Miss detection vs. false alarm: Adversarial learning for small object segmentation in infrared images. In *Proceedings of the IEEE/CVF International Conference on Computer Vision (ICCV)*, 8509–8518.
- Wu, T.; Li, B.; Luo, Y.; Wang, Y.; Xiao, C.; Liu, T.; Yang, J.; An, W.; and Guo, Y. 2023. MTU-Net: Multilevel TransUNet for Space-Based Infrared Tiny Ship Detection. *IEEE Transactions on Geoscience and Remote Sensing*, 61: 1–15.
- Wu, X.; Hong, D.; and Chanussot, J. 2022. UIU-Net: U-Net in U-Net for infrared small object detection. *IEEE Transactions on Image Processing*, 32: 364–376.
- Xu, N.; Price, B.; Cohen, S.; Yang, J.; and Huang, T. S. 2016. Deep interactive object selection. In *Proceedings of the IEEE Conference on Computer Vision and Pattern Recognition (CVPR)*, 373–381.
- Ying, X.; Liu, L.; Wang, Y.; Li, R.; Chen, N.; Lin, Z.; Sheng, W.; and Zhou, S. 2023. Mapping Degeneration Meets Label Evolution: Learning Infrared Small Target Detection with Single Point Supervision. In *Proceedings of the IEEE/CVF Conference on Computer Vision and Pattern Recognition (CVPR)*, 15528–15538.
- Yuan, S.; Qin, H.; Yan, X.; Akhtar, N.; and Mian, A. 2024. SCTransNet: Spatial-channel Cross Transformer Network for Infrared Small Target Detection. *IEEE Transactions on Geoscience and Remote Sensing*, 62: 1–15.
- Zhai, S.; Wang, G.; Luo, X.; Yue, Q.; Li, K.; and Zhang, S. 2023. PA-Seg: Learning From Point Annotations for 3D Medical Image Segmentation Using Contextual Regularization and Cross Knowledge Distillation. *IEEE Transactions on Medical Imaging*, 42(8): 2235–2246.
- Zhang, H.; Burrows, L.; Meng, Y.; Sculthorpe, D.; Mukherjee, A.; Coupland, S. E.; Chen, K.; and Zheng, Y. 2023. Weakly supervised segmentation with point annotations for histopathology images via contrast-based variational model. In *Proceedings of the IEEE/CVF Conference on Computer Vision and Pattern Recognition (CVPR)*, 15630–15640.
- Zhang, M.; Wang, Y.; Guo, J.; Li, Y.; Gao, X.; and Zhang, J. 2024a. IRSAM: Advancing Segment Anything Model for Infrared Small Target Detection. *arXiv preprint arXiv:2407.07520*.
- Zhang, M.; Yang, H.; Guo, J.; Li, Y.; Gao, X.; and Zhang, J. 2024b. IRPruneDet: efficient infrared small target detection via wavelet structure-regularized soft channel pruning. In *Proceedings of the AAAI Conference on Artificial Intelligence*, volume 38, 7224–7232.
- Zhang, M.; Zhang, R.; Yang, Y.; Bai, H.; Zhang, J.; and Guo, J. 2022. ISNet: Shape matters for infrared small target detection. In *Proceedings of the IEEE/CVF Conference on Computer Vision and Pattern Recognition (CVPR)*, 877–886.
- Zhang, S.; Liew, J. H.; Wei, Y.; Wei, S.; and Zhao, Y. 2020. Interactive Object Segmentation With Inside-Outside Guidance. In *2020 IEEE/CVF Conference on Computer Vision and Pattern Recognition (CVPR)*, 12231–12241.
- Zhao, T.; and Yin, Z. 2020. Weakly supervised cell segmentation by point annotation. *IEEE Transactions on Medical Imaging*, 40(10): 2736–2747.